Supplementary Information

Effect of atmospheric water vapor on independent-parallel thermal dehydration of a compacted composite of an inorganic hydrate: sodium carbonate monohydrate grains comprising crystalline particles and a matrix

Yuto Zushi, Shun Iwasaki, and Nobuyoshi Koga*

Department of Science Education, Division of Educational Sciences, Graduate School of Humanities and Social Sciences, Hiroshima University, 1-1-1 Kagamiyama, Higashi-Hiroshima 739-8524, Japan

Contents

* Corresponding author; e-mail: nkoga@hiroshima-u.ac.jp

S1. Physico-geometrical features of the thermal dehydration

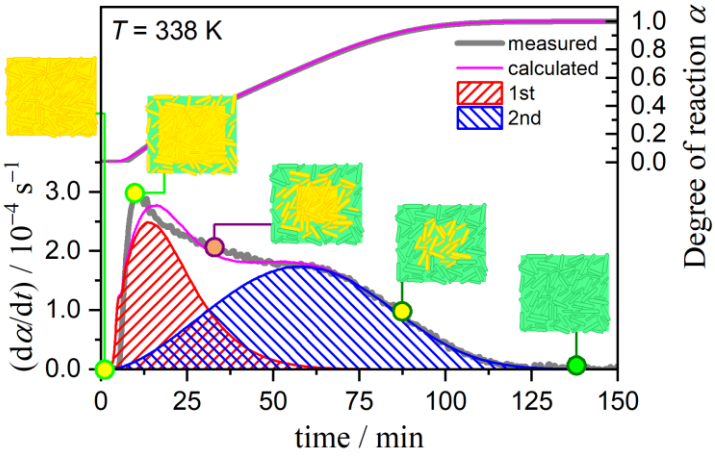

Figure S1. Schematic illustration of the physico-geometrical reaction mechanism of the thermal dehydration of SC-MH in flowing dry N_2, revealed in our previous study.[13]

S2. Influence of $p(H_2O)$ on the kinetics of the IP process

Table S1. Arrhenius parameters for the IP processes at different $p(H_2O)$ values determined using the conventional Arrhenius plot

$p(H_2O)$ / kPa	$E_{a,IP}$ / kJ mol^{-1}	$\ln[A_{IP} \cdot f_{IP}(\alpha_{IP})$ / s$^{-1}]$	$-\gamma$, [a]
0.9	320.1 ± 15.6	106.3 ± 5.5	0.9941
2.6	420.7 ± 7.6	138.3 ± 2.6	0.9992
5.6	525.9 ± 26.2	170.9 ± 8.9	0.9951
10.3	548.1 ± 37.9	175.7 ± 12.6	0.9953

[a] Correlation coefficient of the linear regression analysis.

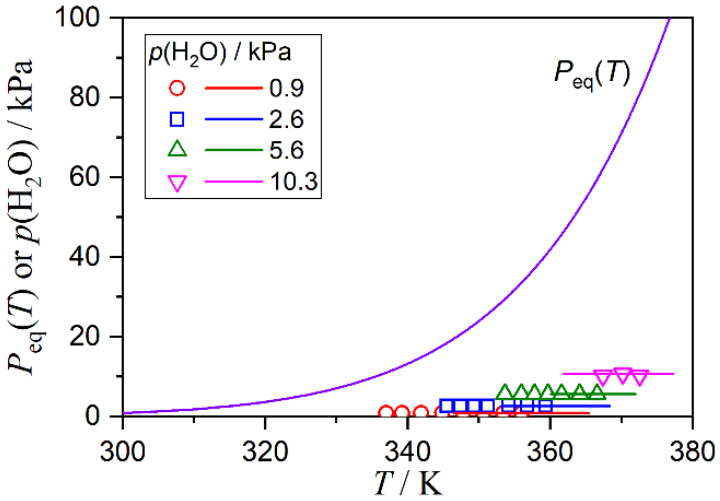

Figure S2. Equilibrium pressure ($P_{eq}(T)$) at different temperatures.

S3. Conventional kinetic analysis of the mass loss process

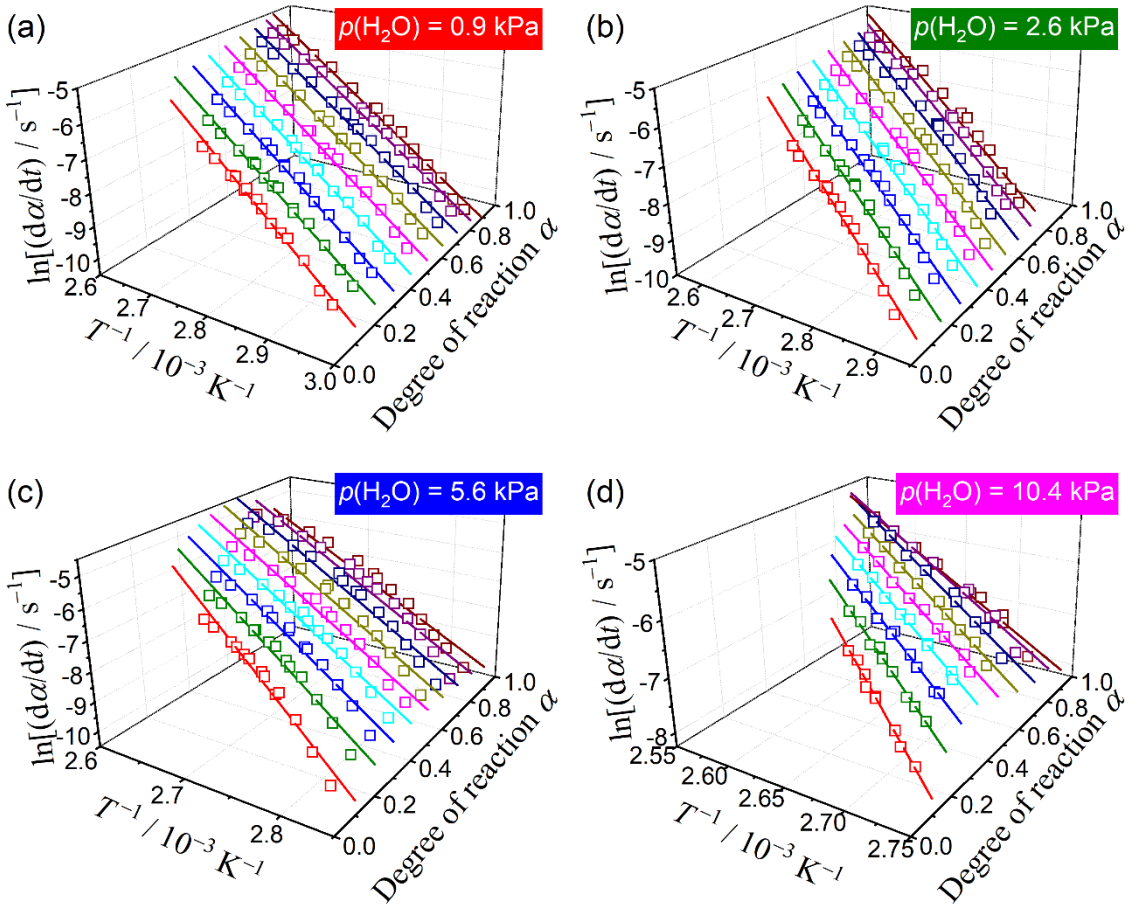

Figure S3. Friedman plots at different α for the overall mass loss process of the thermal dehydration of SC-MH compacted composite at individual $p(H_2O)$ values: (a) 0.9, (b) 2.6, (c) 5.6, and (d) 10.4 kPa.

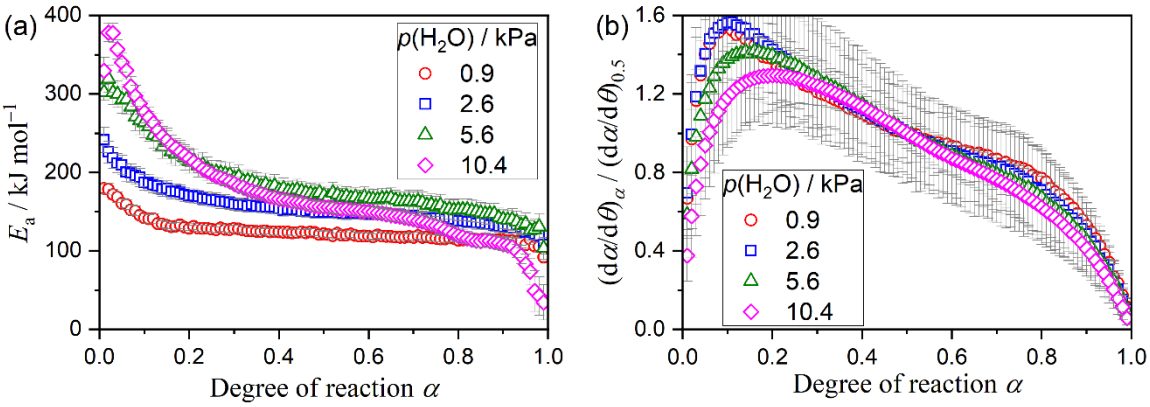

Figure S4. (a) E_a values at different α values and (b) experimental master plots for the overall mass loss process of the thermal dehydration of SC-MH compacted composite at individual $p(H_2O)$ values.

S4. Mathematical deconvolution analysis of the mass loss process

The individual DTG peaks recorded under linear nonisothermal conditions at different $p(H_2O)$ values were deconvoluted into two reaction step based on the cumulative equation of the statistical functions $F(t)$:

$$\frac{dm}{dt} = \sum_{i=1}^{2} F_i(t) \qquad \text{(S1)}$$

After examining fitting using various $F(t)$, the Weibull function was selected as appropriate for the MDA.

■ Weibull function

$$F(t) = a_0\left(\frac{a_3-1}{a_3}\right)^{\frac{1-a_3}{a_3}}\left\{\frac{t-a_1}{a_2}+\left(\frac{a_3-1}{a_3}\right)^{\frac{1}{a_3}}\right\}^{a_3-1}\exp\left[-\left\{\frac{t-a_1}{a_2}+\left(\frac{a_3-1}{a_3}\right)^{\frac{1}{a_3}}\right\}^{a_3}+\frac{a_3-1}{a_3}\right] \quad \text{(S2)}$$

Figure S5 shows the typical results of MDA for the DTG curves at a β of 3 K min^{-1} at different $p(H_2O)$ values. The contributions of the first and second mass loss steps (c_1, c_2) were determined to be approximately (~0.39, ~0.61) from the ratio of peak areas. Table S1 summarizes the results of MDA. The separated DTG curves for the first and second mass loss steps at individual $p(H_2O)$ values (Figures S6–S9) were used to calculate the kinetic parameters to be subsequently used as the initial values for the KDA. For each reaction step, the basic kinetic equation was assumed:

$$\frac{d\alpha}{dt} = A\exp\left(-\frac{E_a}{RT}\right)f(\alpha) \quad \text{(S3)}$$

where A, E_a, R, and $f(\alpha)$ are the Arrhenius preexponential factor, apparent activation energy, gas constant, and the kinetic model function. Taking logarithms of eq. (S3), we obtain eq. (S4).

$$\ln\left(\frac{d\alpha}{dt}\right) = \ln[Af(\alpha)] - \frac{E_a}{RT} \quad \text{(S4)}$$

At a selected α value, the plot of $\ln(d\alpha/dt)$ against T^{-1} (Friedman plot[41]) exhibits a linear correlation for the ideal single-step reaction as described by eq. (S3). The Friedman plots at different α_i values of the first (i = 1) and second (i = 2) reaction steps of the thermal dehydration of SC-MH compacted composite at different $p(H_2O)$ values are shown in Figures S10 and S11, respectively. The Friedman plots showed an approximate linear correlation irrespective of α_i, $p(H_2O)$, and reaction step. However, as the reaction advanced in each reaction step, the slope of the Friedman plots decreased, which was more significantly observed for the first reaction step and at a higher $p(H_2O)$ value. The E_a variation reflected the variation behavior of the Friedman plots as the reaction advanced (Figure S12). In each reaction step, the significant decreasing trend of $E_{a,i}$ values were evident during the first half of the reaction steps. This trend was enhanced with increasing $p(H_2O)$ value followed by the systematic increase in the E_a value with an increase in the $p(H_2O)$ value. In contrast, the E_a values were comparable among those at different $p(H_2O)$ values during the final part of each reaction step.

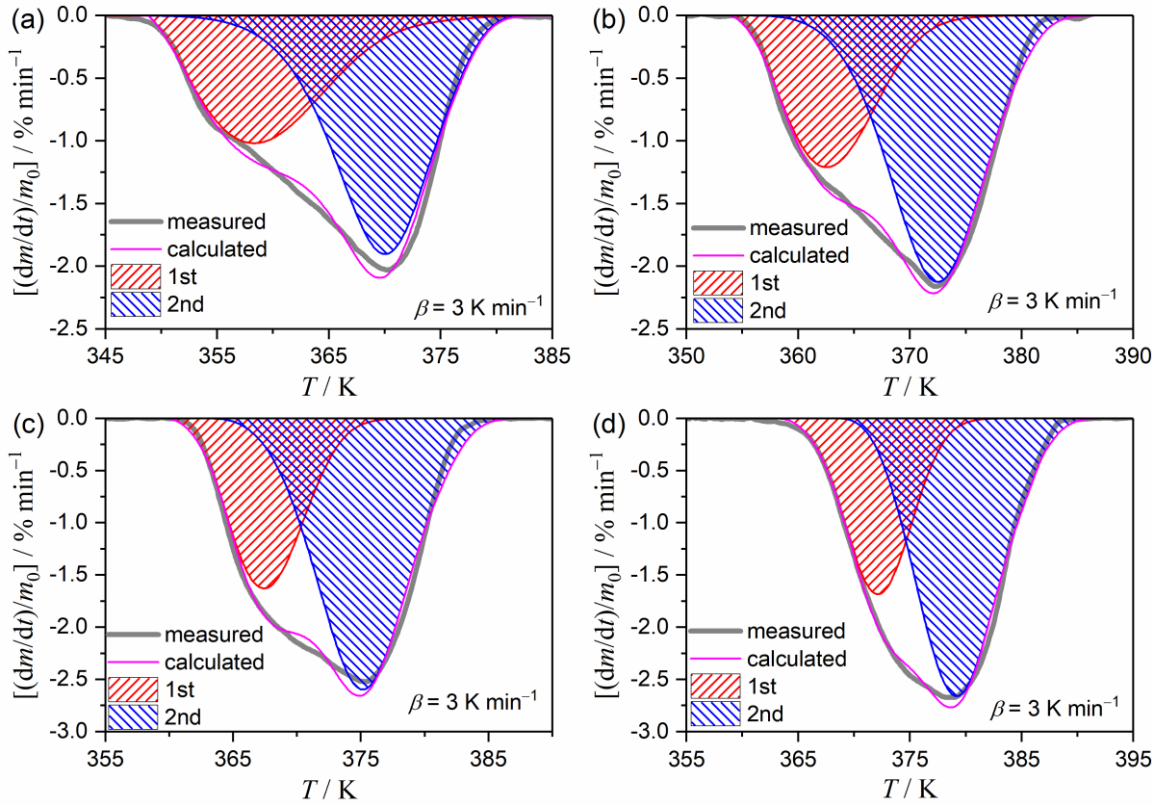

Figure S5. Typical fitting results of the MDA for the mass loss processes under linear nonisothermal conditions at different $p(H_2O)$ values: (a) 0.9, (b) 2.7, (c) 5.6, and (d) 10.4 kPa.

Table S2. The kinetic results for the individual reaction steps of the thermal dehydration of SC-MH under linear nonisothermal conditions determined via MDA and subsequent formal kinetic analysis

$p(H_2O)$ / kPa	i	c_i	$E_{a,i}$ / kJ mol^{-1}, [a]	$\frac{d\alpha_i}{d\theta_i} = A_i\alpha^{m_i}(1-\alpha_i)^{n_i}[-\ln(1-\alpha_i)]^{p_i}$				
				A_i / s^{-1}	m_i	n_i	p_i	$R^{2, b}$
0.9	1	0.40 ± 0.02	106.7 ± 11.7	(2.93 ± 0.03) × 10^{13}	1.63 ± 0.09	0.69 ± 0.03	−1.20 ± 0.09	0.9998
	2	0.60 ± 0.02	94.8 ± 5.6	(2.55 ± 0.01) × 10^{11}	0.10 ± 0.02	1.05 ± 0.01	0.53 ± 0.02	0.9999
2.7	1	0.38 ± 0.02	129.3 ± 12.8	(4.86 ± 0.03) × 10^{16}	1.37 ± 0.06	0.74 ± 0.02	−0.89 ± 0.06	0.9999
	2	0.62 ± 0.02	100.5 ± 9.3	(1.46 ± 0.01) × 10^{12}	0.28 ± 0.03	1.02 ± 0.01	0.34 ± 0.03	0.9999
5.6	1	0.38 ± 0.01	151.2 ± 38.8	(4.03 ± 0.02) × 10^{19}	0.96 ± 0.04	0.81 ± 0.02	−0.44 ± 0.04	0.9999
	2	0.62 ± 0.01	104.1 ± 10.7	(3.92 ± 0.02) × 10^{12}	0.34 ± 0.03	0.99 ± 0.01	0.30 ± 0.03	0.9999
10.4	1	0.39 ± 0.01	204.2 ± 71.9	(6.56 ± 0.04) × 10^{26}	1.10 ± 0.06	0.74 ± 0.02	−0.63 ± 0.05	0.9999
	2	0.61 ± 0.01	126.3 ± 24.6	(3.76 ± 0.02) × 10^{15}	0.58 ± 0.04	0.93 ± 0.02	0.02 ± 0.04	0.9999

[a] Averaged over $0.1 \leq \alpha_i \leq 0.9$.
[b] Determination coefficient of the nonlinear least-squares analysis.

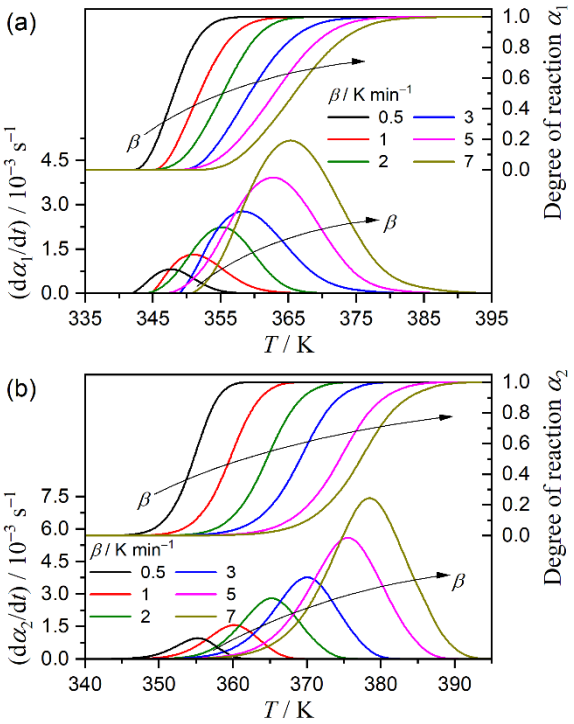

Figure S6. Kinetic curves under linear nonisothermal conditions at different β values for the individual reaction steps of the thermal dehydration of SC-MH at $p(H_2O) = 0.9$ kPa: (a) first and (b) second reaction steps.

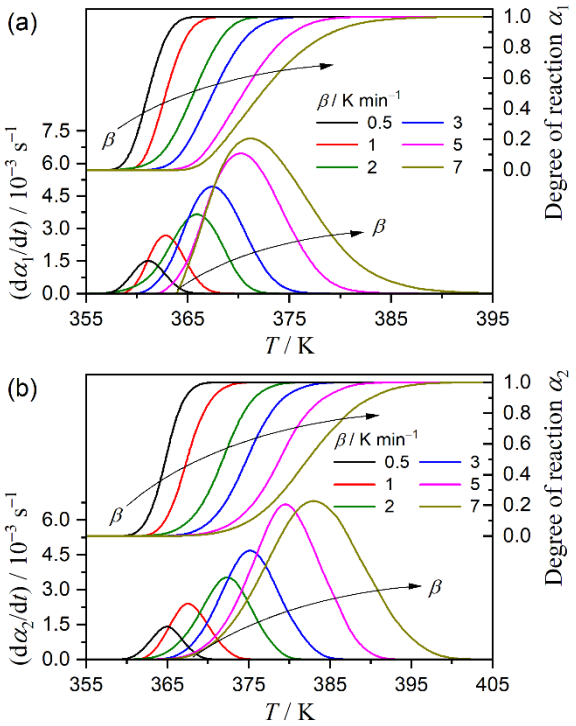

Figure S8. Kinetic curves under linear nonisothermal conditions at different β values for the individual reaction steps of the thermal dehydration of SC-MH at $p(H_2O) = 5.6$ kPa: (a) first and (b) second reaction steps.

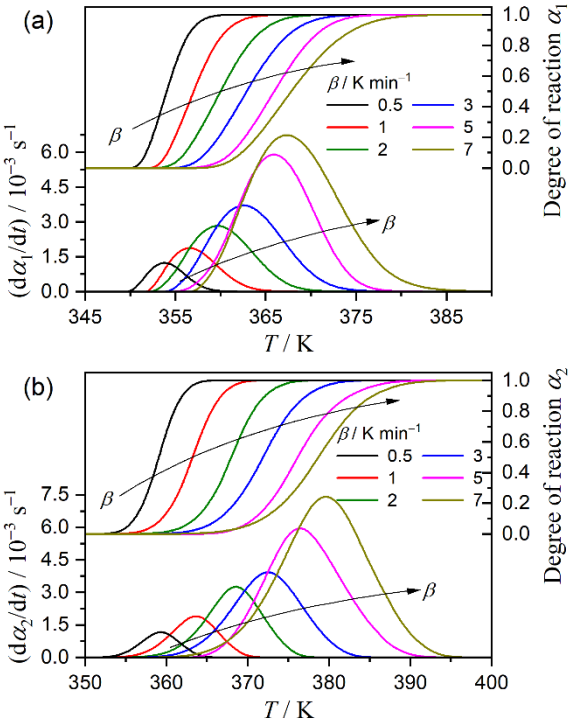

Figure S7. Kinetic curves under linear nonisothermal conditions at different β values for the individual reaction steps of the thermal dehydration of SC-MH at $p(H_2O) = 2.7$ kPa: (a) first and (b) second reaction steps.

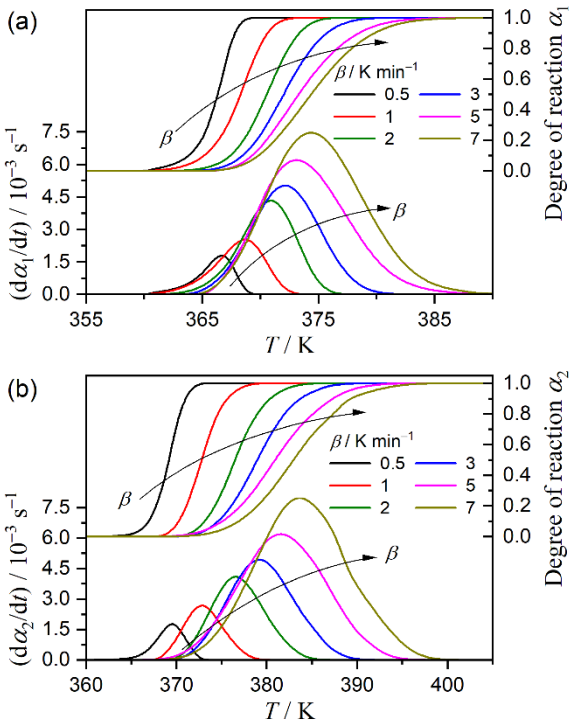

Figure S9. Kinetic curves under linear nonisothermal conditions at different β values for the individual reaction steps of the thermal dehydration of SC-MH at $p(H_2O) = 10.4$ kPa: (a) first and (b) second reaction steps.

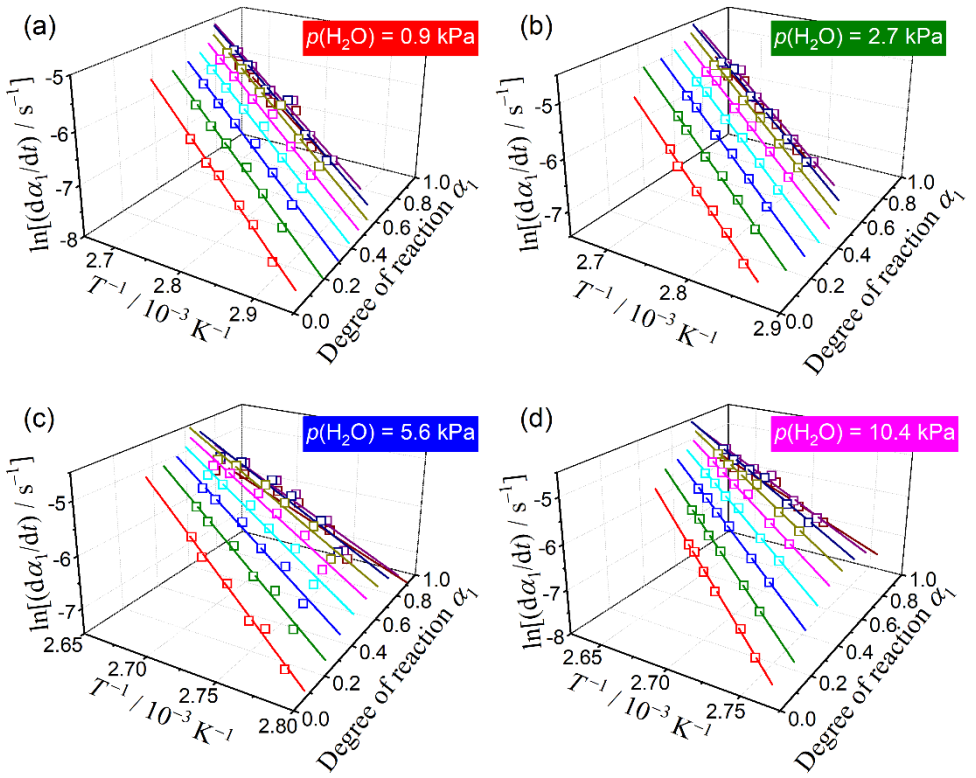

Figure S10. Friedman plots for the first reaction step of the thermal dehydration of SC-MH under linear nonisothermal conditions at different $p(H_2O)$ values: (a) 0.9, (b) 2.7, (c) 5.6, and (d) 10.4 kPa.

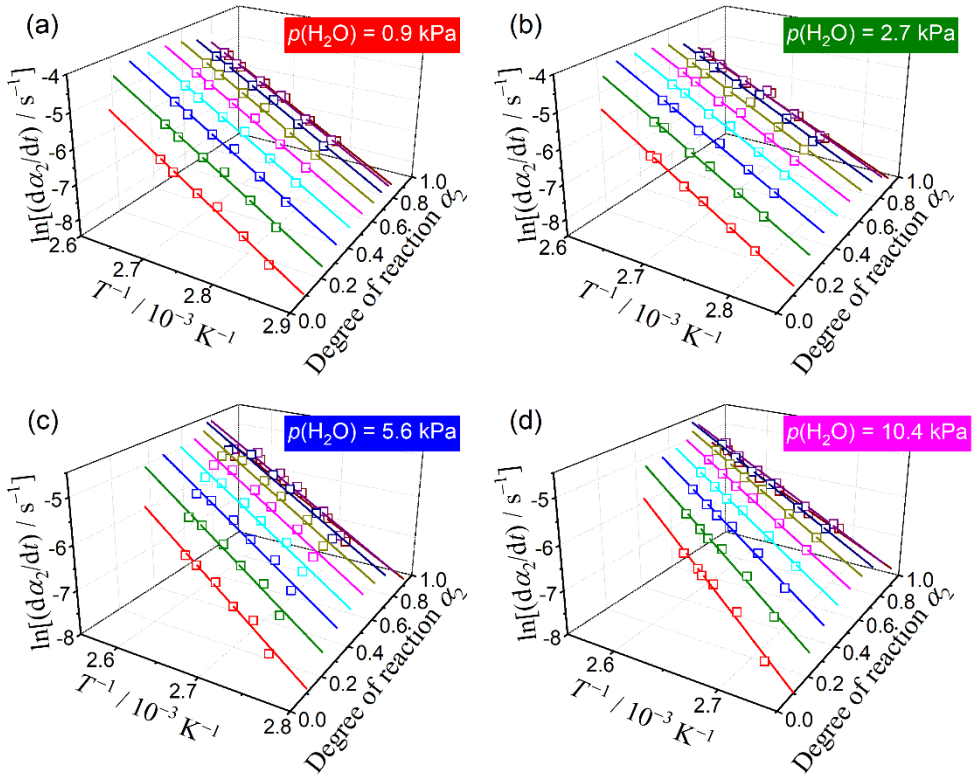

Figure S11. Friedman plots for the second reaction step of the thermal dehydration of SC-MH under linear nonisothermal conditions at different $p(H_2O)$ values: (a) 0.9, (b) 2.7, (c) 5.6, and (d) 10.4 kPa.

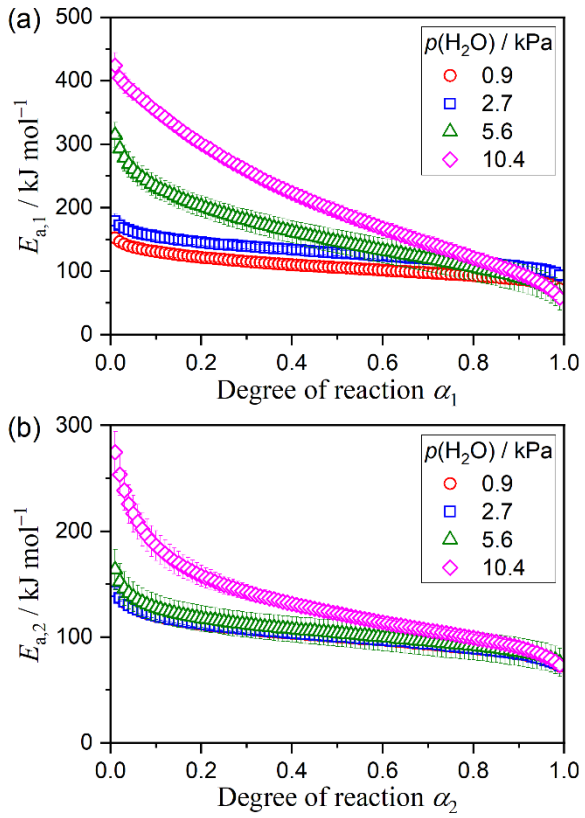

Figure S12. $E_{a,i}$ values at different α_i values for the individual reaction steps of the thermal dehydration of SC-MH at different $p(H_2O)$ values: (a) first (i = 1) and (b) second (i = 2) reaction steps.

The rate behavior at a constant temperature can be described by an experimental master plot for the kinetic process that exhibits a constant E_a during the reaction. At an infinite temperature, the hypothetical reaction rate ($d\alpha/d\theta$) at a selected α can be calculated based on Ozawa's generalized time (θ) concept.[42-48]

$$\frac{d\alpha}{d\theta} = \left(\frac{d\alpha}{dt}\right)\exp\left(\frac{E_a}{RT}\right) = Af(\alpha)$$

$$\text{with} \qquad \theta = \int_0^t \exp\left(-\frac{E_a}{RT}\right)dt \qquad \text{(S5)}$$

The average values of $E_{a,i}$ in the α_i range of 0.1–0.9 (Table S2) were used to calculate $d\alpha_i/d\theta_i$ values at different α_i values as an approximated approach because the $E_{a,i}$ values for both the first and second reaction steps exhibited decreasing trends with increasing α_i value. The normalized experimental master plots of $(d\alpha_i/d\theta_i)_{\alpha(i)}/(d\alpha_i/d\theta_i)_{0.5}$ versus α_i at different $p(H_2O)$ values for the first and second reaction steps are shown in Figure S13. The experimental master plots for the first reaction step (Figure S13(a)) showed the maximum reaction rate in the first-half of the reaction step regardless of the $p(H_2O)$ value. However, the α_1 value at the maximum rate systematically shifted from α_1 = 0.25 at $p(H_2O)$ = 0.9 kPa to α_1 = 0.31 at $p(H_2O)$ = 10.4 kPa. The experimental master plots for the second reaction step (Figure S13(b)) also sowed the maximum rate halfway through the reaction step, irrespective of the $p(H_2O)$ value, and it appeared at approximately the same α_2 value, i.e., 0.43 ± 0.02. According to eq. (S5), the experimental master plots at individual reaction steps and $p(H_2O)$ values were correlated to $A_i f_i(\alpha_i)$ using the empirical kinetic model function of the Šesták–Berggren model (SB(m, n, p)) (eq. (7))[49-51] because of the excellent flexibility fitting various types of physico-geometrical rate behavior at a constant temperature. Each experimental master plot was fitted by optimizing the A_i, m_i, n_i, and p_i values through nonlinear least squares analysis using the Levenberg-Marquart algorithm. The optimized values of A_i, m_i, n_i, and p_i values for each reaction step and $p(H_2O)$ value are listed in Table S2, which were used as the initial values for further optimization via KDA.

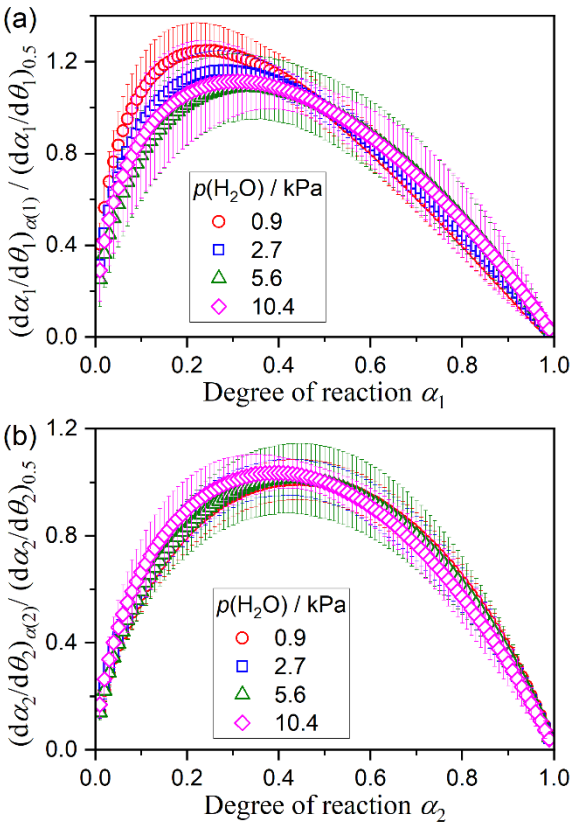

Figure S13. The experimental master plots of $(d\alpha_i/d\theta_i)_{\alpha(i)}/(d\alpha_i/d\theta_i)_{0.5}$ values α_i for the individual reaction steps of the thermal dehydration of SC-MH at different $p(H_2O)$ values: (a) first (i = 1) and (b) second (i = 2) reaction steps.

S5. Kinetic deconvolution analysis of the mass loss process

Table S3. The kinetic parameters optimized via KDA and averaged over those at different β values for individual reaction steps of the thermal dehydration of SC-MH under linear nonisothermal conditions at different $p(H_2O)$ values

$p(H_2O)$ / kPa	Step i	c_i	$E_{a,i}$ / kJ mol^{-1}	A_i / s^{-1}	m_i	n_i	p_i	$R^{2,a}$
0.9	1	0.35 ± 0.05	105.7 ± 0.6	(2.94 ± 0.05) × 10^{13}	1.89 ± 0.12	0.77 ± 0.07	−1.19 ± 0.06	0.9965 ± 0.0011
	2	0.65 ± 0.05	94.9 ± 0.6	(2.32 ± 0.28) × 10^{11}	0.10 ± 0.01	0.94 ± 0.09	0.56 ± 0.07	
2.7	1	0.34 ± 0.05	128.2 ± 0.8	(4.80 ± 0.17) × 10^{16}	1.67 ± 0.11	1.00 ± 0.28	−0.91 ± 0.11	0.9963 ± 0.0014
	2	0.66 ± 0.05	100.6 ± 0.4	(1.38 ± 0.14) × 10^{12}	0.32 ± 0.04	0.94 ± 0.06	0.38 ± 0.06	
5.6	1	0.36 ± 0.04	150.1 ± 1.1	(3.94 ± 0.15) × 10^{19}	1.21 ± 0.05	1.14 ± 0.36	−0.43 ± 0.05	0.9968 ± 0.0010
	2	0.64 ± 0.04	103.9 ± 0.6	(3.64 ± 0.38) × 10^{12}	0.41 ± 0.05	0.97 ± 0.13	0.35 ± 0.05	
10.4	1	0.37 ± 0.04	202.7 ± 1.8	(7.33 ± 0.49) × 10^{26}	1.51 ± 0.12	1.25 ± 0.51	−0.62 ± 0.06	0.9943 ± 0.0062
	2	0.63 ± 0.04	125.2 ± 1.4	(3.47 ± 0.45) × 10^{15}	0.89 ± 0.04	1.05 ± 0.32	0.02 ± 0.01	

[a] Determination coefficient of the nonlinear least-squares analysis.

Table S4. The kinetic parameters optimized via KDA and averaged over those at different temperatures for individual reaction steps of the thermal dehydration of SC-MH under isothermal conditions at different $p(H_2O)$ values

$p(H_2O)$ / kPa	Step i	c_i	$E_{a,i}$ / kJ mol$^{-1,a}$	A_i / s^{-1}	m_i	n_i	p_i	$R^{2,a}$
0.9	1	0.35 ± 0.02	106.3 ± 1.2	(2.89 ± 0.12) × 10^{13}	1.90 ± 0.09	0.80 ± 0.08	−1.23 ± 0.09	0.9941 ± 0.0018
	2	0.65 ± 0.02	96.1 ± 1.1	(2.18 ± 0.16) × 10^{11}	0.10 ± 0.01	0.88 ± 0.07	0.51 ± 0.03	
2.6	1	0.35 ± 0.04	129.5 ± 1.9	(4.77 ± 0.03) × 10^{16}	1.65 ± 0.10	1.05 ± 0.18	−0.94 ± 0.06	0.9940 ± 0.0013
	2	0.65 ± 0.04	102.9 ± 1.8	(1.29 ± 0.10) × 10^{12}	0.27 ± 0.02	0.81 ± 0.10	0.32 ± 0.02	
5.6	1	0.37 ± 0.02	151.7 ± 2.4	(3.86 ± 0.12) × 10^{19}	1.15 ± 0.07	1.13 ± 0.22	−0.44 ± 0.02	0.9959 ± 0.0010
	2	0.63 ± 0.02	106.6 ± 2.0	(3.48 ± 0.11) × 10^{12}	0.33 ± 0.02	0.82 ± 0.06	0.30 ± 0.02	
10.4	1	0.39 ± 0.02	203.5 ± 0.6	(7.24 ± 0.03) × 10^{26}	1.36 ± 0.03	1.03 ± 0.13	−0.62 ± 0.02	0.9961 ± 0.0003
	2	0.61 ± 0.02	126.6 ± 0.7	(3.28 ± 0.07) × 10^{15}	0.72 ± 0.02	0.73 ± 0.03	0.02 ± 0.01	

[a] Determination coefficient of the nonlinear least-squares analysis.

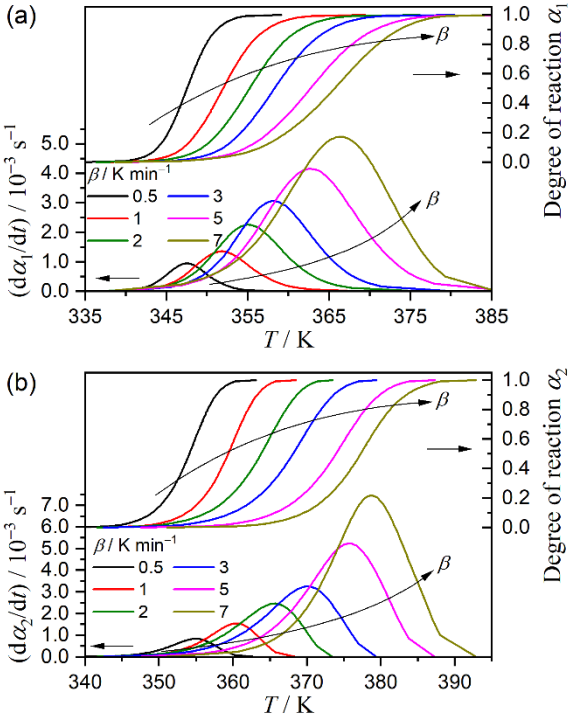

Figure S14. Kinetic curves for each reaction step of the thermal dehydration of SC-MH under nonisothermal conditions at $p(H_2O)$ = 0.9 kPa obtained by KDA: (a) first and (b) second reaction steps.

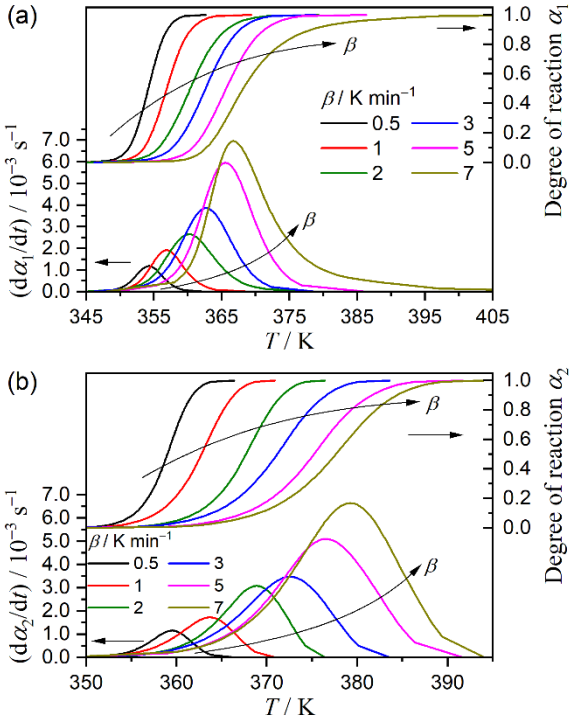

Figure S16. Kinetic curves for each reaction step of the thermal dehydration of SC-MH under nonisothermal conditions at $p(H_2O)$ = 2.6 kPa obtained by KDA: (a) first and (b) second reaction steps.

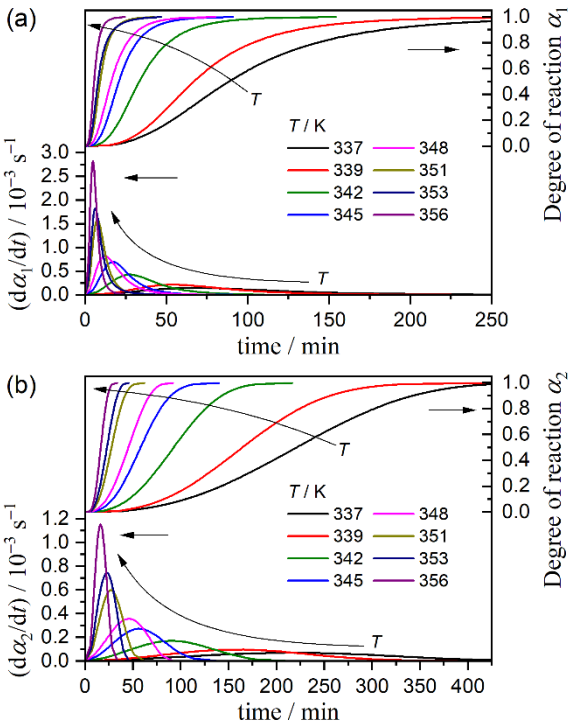

Figure S15. Kinetic curves for each reaction step of the thermal dehydration of SC-MH under isothermal conditions at $p(H_2O)$ = 0.9 kPa obtained by KDA: (a) first and (b) second reaction steps.

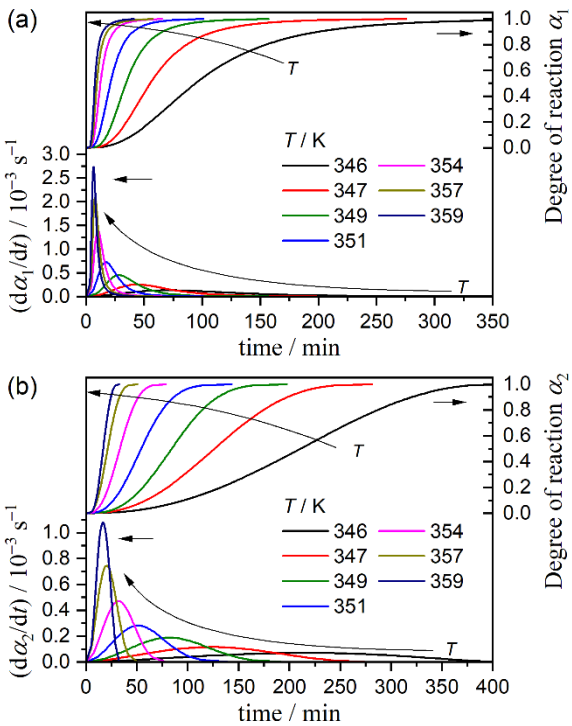

Figure S17. Kinetic curves for each reaction step of the thermal dehydration of SC-MH under isothermal conditions at $p(H_2O)$ = 2.6 kPa obtained by KDA: (a) first and (b) second reaction steps.

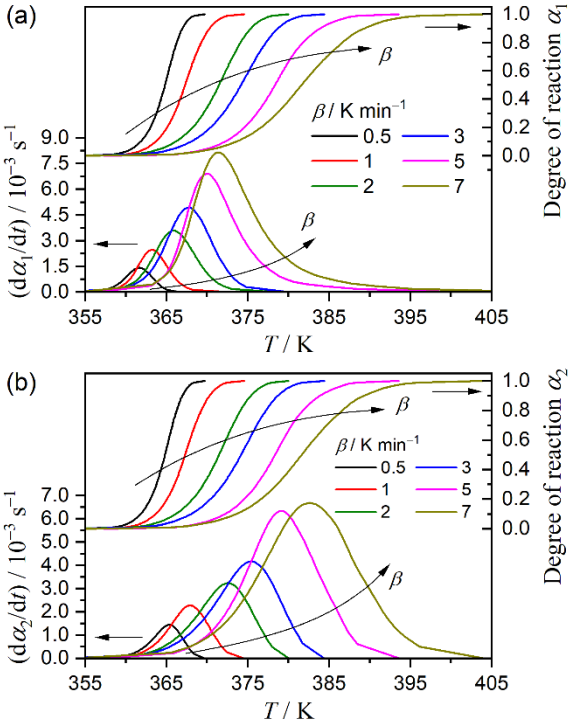

Figure S18. Kinetic curves for each reaction step of the thermal dehydration of SC-MH under nonisothermal conditions at $p(H_2O)$ = 5.6 kPa obtained by KDA: (a) first and (b) second reaction steps.

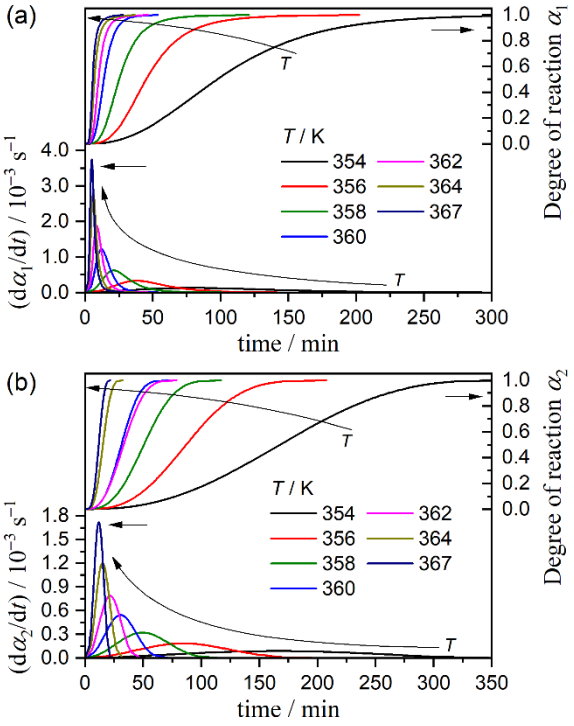

Figure S19. Kinetic curves for each reaction step of the thermal dehydration of SC-MH under isothermal conditions at $p(H_2O)$ = 5.6 kPa obtained by KDA: (a) first and (b) second reaction steps.

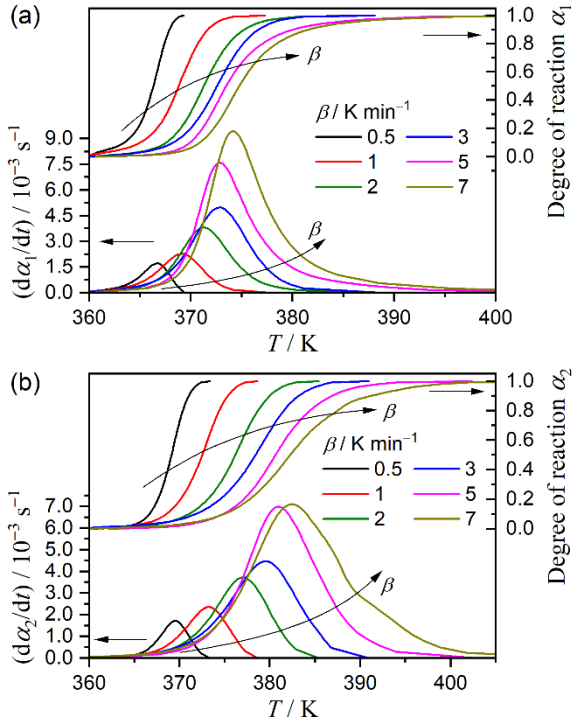

Figure S20. Kinetic curves for each reaction step of the thermal dehydration of SC-MH under nonisothermal conditions at $p(H_2O)$ = 10.4 kPa obtained by KDA: (a) first and (b) second reaction steps.

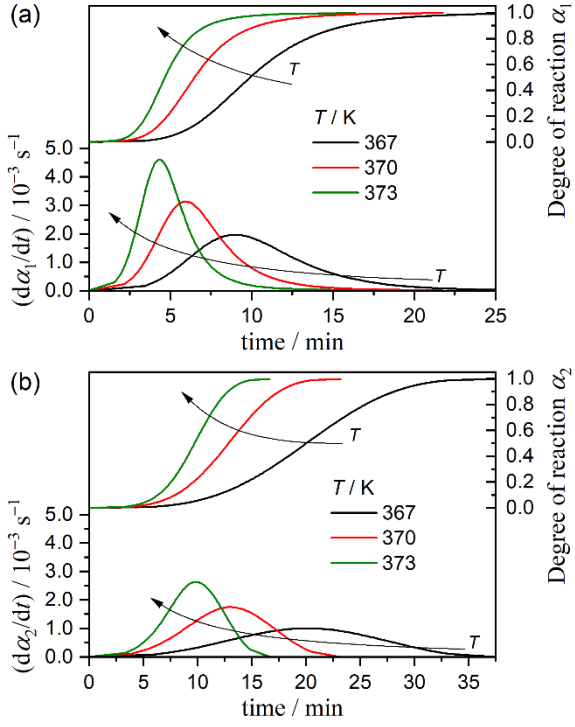

Figure S21. Kinetic curves for each reaction step of the thermal dehydration of SC-MH under isothermal conditions at $p(H_2O)$ = 10.4 kPa obtained by KDA: (a) first and (b) second reaction steps.

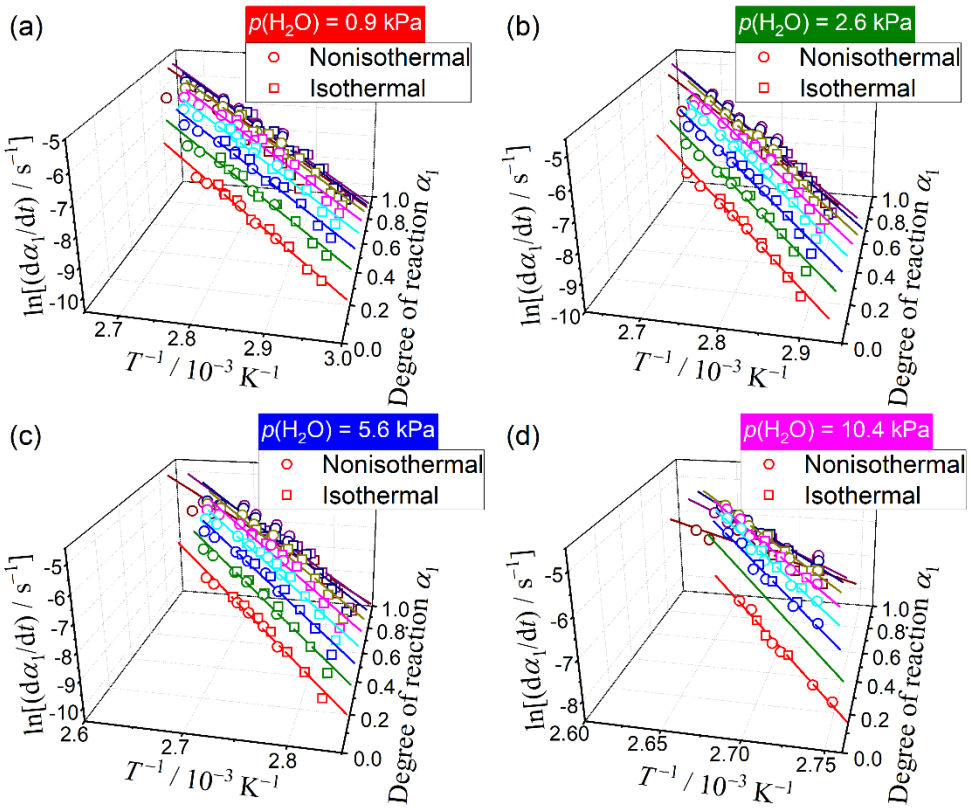

Figure S22. Friedman plots for the first reaction step at each $p(H_2O)$ value using the kinetic data obtained by KDA: $p(H_2O)$ = (a) 0.9, (b) 2.6, (c) 5.6, and (d) 10.4 kPa.

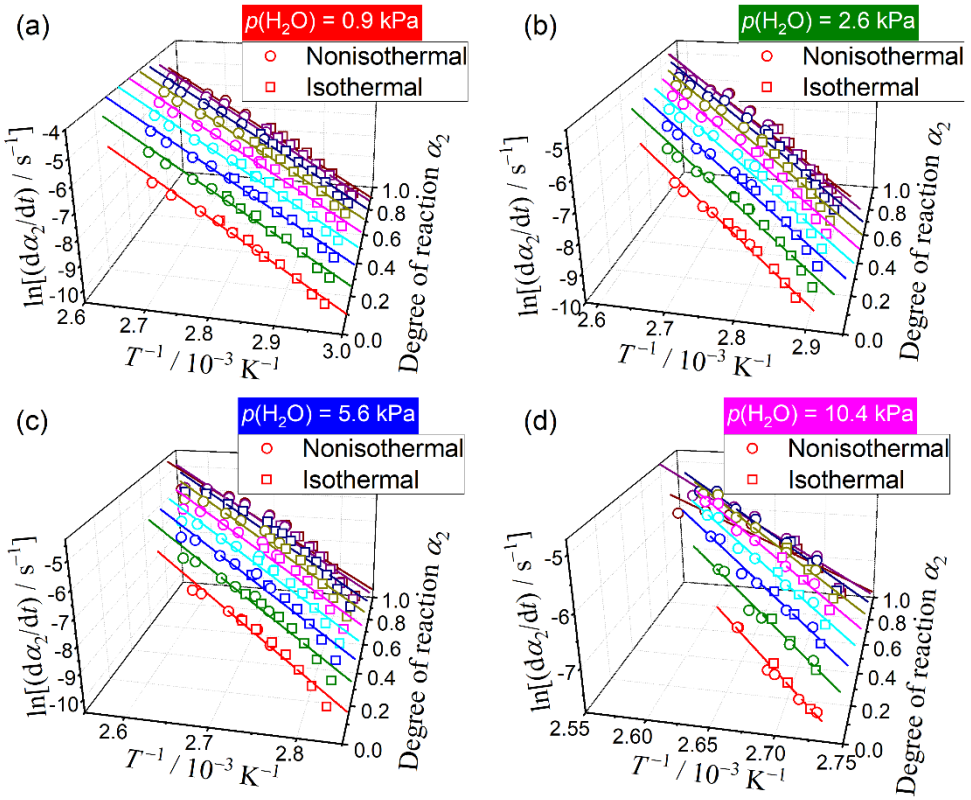

Figure S23. Friedman plots for the second reaction step at each $p(H_2O)$ value using the kinetic data obtained by KDA: $p(H_2O)$ = (a) 0.9, (b) 2.6, (c) 5.6, and (d) 10.4 kPa.

Table S5. Results of conventional kinetic analysis by the isoconversional and master plot methods applied to the kinetic data of each reaction step at individual $p(H_2O)$ values obtained by KDA

i	$p(H_2O)$ / kPa	$E_{a,i}$ / kJ mol^{-1}, [a]	$\frac{d\alpha_i}{d\theta_i} = A_i\alpha^{m_i}(1-\alpha_i)^{n_i}[-\ln(1-\alpha_i)]^{p_i}$				
			A_i / s^{-1}	m_i	n_i	p_i	R^{2,b}
1	0.9	132.8 ± 8.2	(2.77 ± 0.02) × 10^{17}	1.70 ± 0.06	0.85 ± 0.03	−1.07 ± 0.06	0.9999
	2.6	181.6 ± 18.2	(2.65 ± 0.01) × 10^{24}	2.24 ± 0.04	0.76 ± 0.02	−1.55 ± 0.04	0.9999
	5.6	232.9 ± 32.4	(2.49 ± 0.01) × 10^{31}	1.99 ± 0.04	0.76 ± 0.02	−1.30 ± 0.04	0.9999
	10.4	228.8 ± 72.5	(3.10 ± 0.03) × 10^{30}	2.77 ± 0.14	0.55 ± 0.06	−1.99 ± 0.13	0.9998
2	0.9	119.1 ± 3.2	(6.34 ± 0.01) × 10^{14}	0.03 ± 0.02	0.92 ± 0.01	0.55 ± 0.02	0.9999
	2.6	146.7 ± 9.2	(4.29 ± 0.01) × 10^{18}	0.18 ± 0.02	0.90 ± 0.01	0.40 ± 0.02	0.9999
	5.6	168.6 ± 14.9	(3.65 ± 0.01) × 10^{21}	0.25 ± 0.02	0.90 ± 0.01	0.36 ± 0.02	0.9999
	10.4	143.6 ± 31.1	(1.03 ± 0.01) × 10^{15}	1.21 ± 0.06	0.72 ± 0.02	−0.43 ± 0.06	0.9999

[a] Averaged over $0.1 \le \alpha_i \le 0.9$.
[b] Determination coefficient of the nonlinear least-squares analysis.

S6. Effect of $p(H_2O)$ on the kinetics of the mass loss process

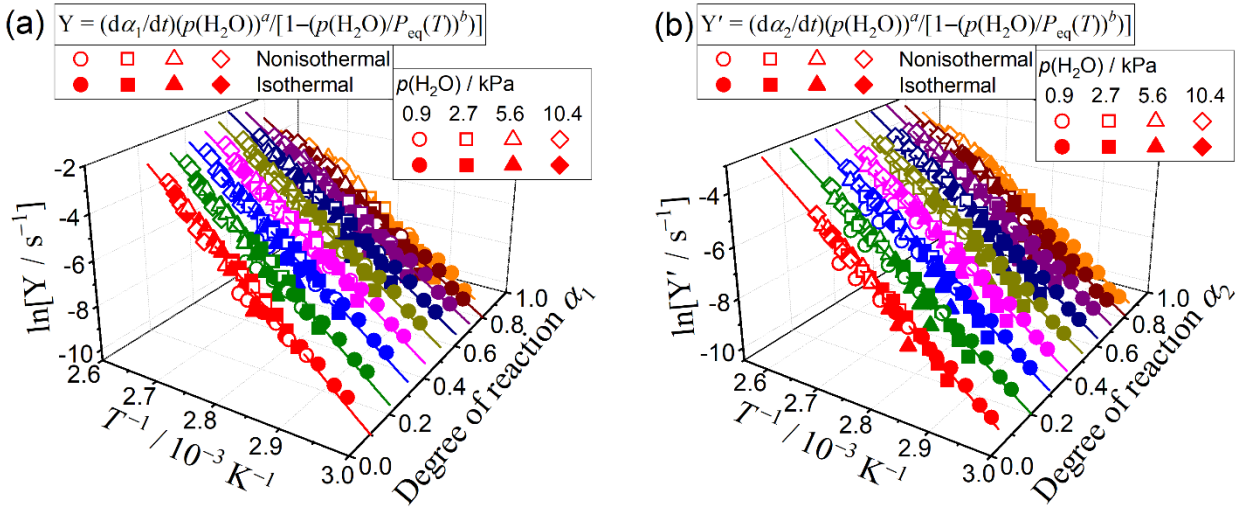

Figure S24. The extended Friedman plots for the separated reaction steps of the thermal dehydration of the SC-MH compacted composite over different $p(H_2O)$ values: (a) first and (b) second reaction steps.

Table S6. The k_{SR} and $k_{PBR(3)}$ values for the first reaction step of the thermal dehydration of the SC-MH compacted composite at different temperatures and $p(H_2O)$ values

$p(H_2O)$/kPa	T / K	k_{SR} / 10^{-3} s^{-1}	$k_{PBR(3)}$ / 10^{-3} s^{-1}	$R^{2,a}$	
				Diff.	Int.
0.9	337	0.34	0.10	0.9918	0.9994
	339	0.49	0.15	0.9911	0.9995
	342	0.86	0.39	0.9978	0.9994
	345	1.43	0.61	0.9971	0.9995
	348	1.56	0.79	0.9985	0.9997
	351	3.06	1.59	0.9976	0.9994
	353	3.14	2.23	0.9963	0.9992
	356	5.80	2.64	0.9944	0.9990
2.6	346	0.31	0.10	0.9941	0.9994
	347	0.70	0.20	0.9956	0.9997
	349	1.35	0.39	0.9946	0.9998
	351	2.53	0.66	0.9969	0.9998
	354	3.88	1.35	0.9961	0.9996
	357	5.36	2.46	0.9954	0.9992
	359	7.91	3.42	0.9943	0.9988
5.6	354	0.30	0.09	0.9915	0.9993
	356	0.70	0.28	0.9979	0.9995
	358	1.35	0.48	0.9939	0.9997
	360	2.53	1.07	0.9984	0.9993
	362	3.88	1.57	0.9947	0.9997
	364	5.36	3.24	0.9971	0.9993
	367	7.91	4.41	0.9956	0.9992
10.4	367	4.40	1.52	0.9942	0.9988
	370	6.76	2.30	0.9974	0.9999
	373	11.27	3.93	0.9878	0.9994

[a]Determination coefficient of the nonlinear least-squares analysis.

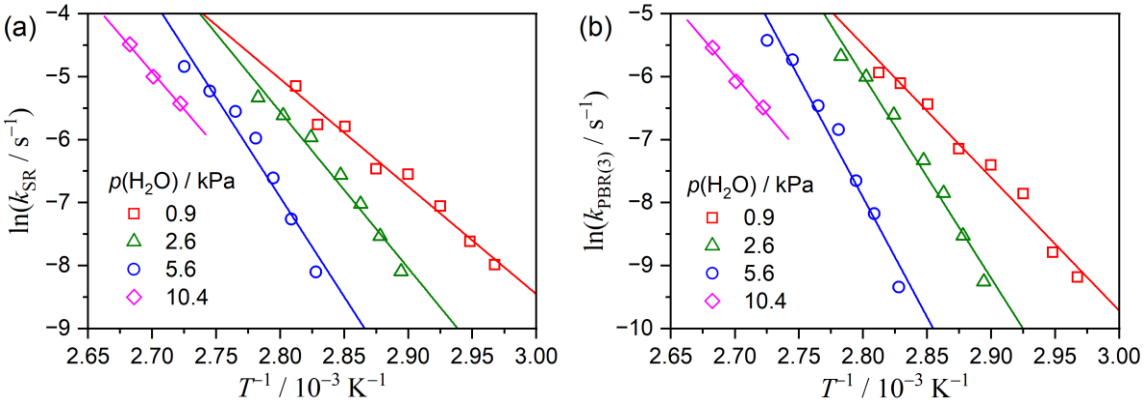

Figure S25. Conventional Arrhenius plots for the individual physico-geometrical processes of the first reaction step of the thermal dehydration of SC-MH compacted composite under isothermal conditions at different $p(H_2O)$ values: (a) SR and (b) PBR(3) processes.